



UNIVERSITY OF LEEDS

This is a repository copy of *Trilobite extinctions, facies changes and the ROECE carbon isotope excursion at the Cambrian Series 2 - 3 boundary, Great Basin, western USA*.

White Rose Research Online URL for this paper:  
<http://eprints.whiterose.ac.uk/115157/>

Version: Accepted Version

---

**Article:**

Faggetter, LE, Wignall, PB, Pruss, SB et al. (3 more authors) (2017) Trilobite extinctions, facies changes and the ROECE carbon isotope excursion at the Cambrian Series 2 - 3 boundary, Great Basin, western USA. *Palaeogeography, Palaeoclimatology, Palaeoecology*, 478. pp. 53-66. ISSN 0031-0182

<https://doi.org/10.1016/j.palaeo.2017.04.009>

---

© 2017, Elsevier. Licensed under the Creative Commons Attribution-NonCommercial-NoDerivatives 4.0 International  
<http://creativecommons.org/licenses/by-nc-nd/4.0/>

**Reuse**

Unless indicated otherwise, fulltext items are protected by copyright with all rights reserved. The copyright exception in section 29 of the Copyright, Designs and Patents Act 1988 allows the making of a single copy solely for the purpose of non-commercial research or private study within the limits of fair dealing. The publisher or other rights-holder may allow further reproduction and re-use of this version - refer to the White Rose Research Online record for this item. Where records identify the publisher as the copyright holder, users can verify any specific terms of use on the publisher's website.

**Takedown**

If you consider content in White Rose Research Online to be in breach of UK law, please notify us by emailing [eprints@whiterose.ac.uk](mailto:eprints@whiterose.ac.uk) including the URL of the record and the reason for the withdrawal request.



[eprints@whiterose.ac.uk](mailto:eprints@whiterose.ac.uk)  
<https://eprints.whiterose.ac.uk/>

1 Trilobite extinctions, facies changes and the ROECE carbon isotope excursion at the  
2 Cambrian Series 2 - 3 boundary, Great Basin, western USA.

3 Faggetter, Luke E.<sup>a</sup>; Wignall, Paul B.<sup>a</sup>; Pruss, Sara B.<sup>b</sup>; Newton, Robert J.<sup>a</sup>; Sun, Yadong<sup>c</sup>; Crowley,  
4 Stephen<sup>d</sup>;

5 <sup>a</sup>The School of Earth and Environment, the University of Leeds, Leeds, West Yorkshire, LS2 9JT,  
6 United Kingdom. [ee08lef@leeds.ac.uk](mailto:ee08lef@leeds.ac.uk); [P.B.Wignall@leeds.ac.uk](mailto:P.B.Wignall@leeds.ac.uk); [r.j.newton@leeds.ac.uk](mailto:r.j.newton@leeds.ac.uk); <sup>b</sup>

7 Department of Geosciences, Smith College, Northampton, MA 01063, United States.

8 [spruss@smith.edu](mailto:spruss@smith.edu); <sup>c</sup> School of Geography and Earth Sciences, Friedrich-Alexander University

9 Erlangen-Nürnberg, Schloßgarten 5, 91054 Erlangen, Germany. [yadong.sun@cug.edu.cn](mailto:yadong.sun@cug.edu.cn); <sup>d</sup> School of

10 Environmental Sciences, University of Liverpool, Jane Herdman Building, Liverpool L69 3GP, United

11 Kingdom. [sfcrow@liverpool.ac.uk](mailto:sfcrow@liverpool.ac.uk).

12 Corresponding author: Luke Faggetter, [ee08lef@leeds.ac.uk](mailto:ee08lef@leeds.ac.uk).

13

14 Abstract

15 The mass extinction of the olenellid trilobites occurred around the Cambrian Series 2 - Series 3  
16 boundary. Like many other crises, it coincided with a negative carbon isotope excursion but the  
17 associated palaeoenvironmental changes remain unclear. To investigate the causal mechanism for  
18 this event, we report facies changes, pyrite framboid petrography and carbon isotope values from  
19 Cambrian Series 2 - Series 3 (traditionally Early - Middle Cambrian) boundary strata of the Carrara  
20 Formation (Death Valley region, California) and Pioche Formation (Nevada). These data reveal  
21 regionally changing water depths from high-energy, nearshore facies (oolitic grainstone) to more  
22 offshore silty marl and finer-grained carbonate mudstone. In the Carrara Formation, the series  
23 boundary occurs within a deepening succession, transitioning from high-energy, nearshore facies  
24 (oolitic grainstone and oncolitic packstone) to offshore marl, the latter of which contains pyrite

25 frambooid populations indicative of low-oxygen (dysoxic) depositional conditions. Intermittent  
26 dysoxia persisted below sub-wave base settings throughout the early and middle Cambrian, but did  
27 not intensify at the time of extinction, arguing against anoxia as a primary cause in the olenellid  
28 trilobite extinction. Within both field areas, the extinction interval coincided with a minimum in  
29  $\delta^{13}\text{C}_{\text{carb}}$  values, which we interpret as the regional manifestation of the Redlichiid-Olenellid Extinction  
30 Carbon isotope Excursion (ROECE). The Series 2 - Series 3 boundary is reported to closely coincide  
31 with a large-amplitude sea-level fall that produced the Sauk I/II sequence boundary, but the  
32 placement of the Series 2 - Series 3 boundary within a transgressive interval of the Carrara  
33 Formation shows that this is not the case. The main sequence boundary in the succession occurs  
34 much lower in the succession (at the top of the Zabriskie Quartzite) and therefore precedes the  
35 extinction of the olenellids and ROECE.

36 Keywords: Olenellid extinction, Carrara Formation, Pyramid Shale Member, Pioche Formation, C-  
37 Shale Member

38

## 39 1. Introduction

40 The first major biotic crisis of the Phanerozoic occurred during the Cambrian Series 2, an  
41 interval that saw the collapse of archaeocyathan reefs (Newell, 1972; Boucot, 1990; Debrenne, 1991;  
42 Zhuravlev and Wood, 1996). This was followed, at the Series 2 - Series 3 boundary, by severe  
43 generic-level losses of olenellid and redlichiid trilobites (Palmer, 1998; Zhu et al., 2004; Zhu et al.,  
44 2006; Fan et al., 2011; Wang et al., 2011; Zhang et al., 2013). This trilobite extinction has been used  
45 to delineate the Series 2 - Series 3 boundary; however, the boundary remains unratiated as  
46 international correlation is confounded by a lack of globally-distributed taxa at this time (Sundberg  
47 et al., 2016). The trilobite extinction coincides with a major negative  $\delta^{13}\text{C}$  excursion that has been  
48 termed the Redlichiid-Olenellid Extinction Carbon Isotope Excursion or ROECE (Zhu et al. 2004,  
49 2006).

50 In the western Great Basin of the United States, a Cambrian sedimentary succession  
51 developed on a rapidly subsiding passive margin (Prave, 1999; Stewart, 1972; Fedo and Cooper,  
52 2001; Hogan et al., 2011; Keller et al., 2012; Morgan, 2012). Sections in the southern Nopah Ranges  
53 (Keller et al., 2012) expose strata from Cambrian Sauk I and Sauk II supersequences that are of  
54 importance to this study (Prave, 1991). These are widespread, large-scale Laurentian sequences that  
55 provide a regional stratigraphic framework. The transition from Sauk I to Sauk II records a major  
56 lithological change that saw the siliciclastic deposition of the Zabriskie Quartzite replaced by  
57 carbonate deposition of the Carrara Formation (Keller et al., 2012; Morgan, 2012). The contact  
58 between these two units is considered to be the Sauk I/II sequence boundary (Keller et al., 2012;  
59 Morgan, 2012).

60 Throughout the Phanerozoic the relationship between environmental perturbation and  
61 extinction is a common focus of studies, including those in the Cambrian (Hallam and Wignall, 1997;  
62 Wignall, 2015). In particular, sea-level change, marine anoxia, carbon isotope excursions and  
63 eruptions of LIPs (large igneous provinces) often coincide with mass extinctions (Zhuravlev and  
64 Wood, 1996; Wignall, 2001; Glass and Phillips, 2006; Jourdan et al., 2014). Thus, Zhuravlev and  
65 Wood (1996) noted the temporal link between widespread deposition of black shales and the  
66 disappearance of the archaeocyathans in the Cambrian of Siberia, and trilobite extinctions at  
67 “biomere” boundaries are also ascribed to dysoxia (Palmer, 1984). However, the role of anoxia in  
68 Cambrian extinctions has to be viewed in the context of persistently oxygen-restricted oceans at this  
69 time (e.g. Montañez et al., 2000; Hurtgen et al., 2009; Pruss et al., 2010; Gill et al., 2011; Saltzman et  
70 al., 2015; Tarhan et al., 2015).

71 Volcanism may also have played a role in ROECE (Glass and Phillips, 2006). The Kalkarindji  
72 LIP is a Cambrian flood basalt province of northern and central Australia with an estimated original  
73 surface area of  $\sim 2.1 \times 10^6 \text{ km}^2$  (Glass and Phillips, 2006; Jourdan et al., 2014; Marshall et al., 2016).

74 Latest dating efforts yield a zircon age of  $510.7 \pm 0.6$  Ma, which is close to that of the Cambrian  
75 Series 2 - Series 3 boundary (Jourdan et al., 2014).

76 In order to improve our understanding of the events associated with ROECE, this study  
77 examines sections spanning the Cambrian Series 2 - Series 3 boundary interval in the western Great  
78 Basin. The olenellid extinction horizon has been located within the Pioche Formation in Nevada  
79 (Palmer, 1998). We have examined this level and the correlative levels in the Carrara Formation in  
80 California in order to examine changes of lithofacies, carbon isotope variability and pyrite  
81 petrography.

82

## 83 **2. Geological background and biostratigraphy**

84 Following breakup of the Rodinia supercontinent in the late Neoproterozoic, the  
85 northwestern margin of Laurentia subsided rapidly (Bond and Kominz, 1984; Levy and Christie-Blick,  
86 1991; Prave, 1999; Howley et al., 2006). By the early Cambrian, the western Great Basin (USA) was  
87 positioned along the western margin of Laurentia where a wide, clastic-dominated shelf developed  
88 in an equatorial setting (Palmer and Halley, 1979; MacNiocaill and Smethurst, 1994; Fig. 1). Clastic  
89 input decreased in late Series 2 and was replaced by carbonate deposition (Erdtmann and Miller,  
90 1981; Howley et al., 2006; Landing, 2012).

91 We have assessed environmental conditions across the Series 2 - Series 3 boundary from  
92 sections in the Great Basin including Emigrant Pass (Nopah Range, Death Valley, eastern California),  
93 and Oak Springs Summit (Burnt Springs Range, eastern Nevada; Fig. 1). The regional lithostratigraphy  
94 of the Pioche Formation (at Oak Springs Summit) was described in detail by Merriam and Palmer  
95 (1964), and the Carrara Formation (at Emigrant Pass) by Palmer and Halley (1979). In addition, we  
96 examined a section of the Pioche Formation at Ruin Wash in eastern Nevada.

97

98 2.1. *Emigrant Pass*

99           At Emigrant Pass the Zabriskie Quartzite and Carrara Formation are easily accessible and  
100 well exposed. The strata are seen on the north side of Old Spanish Trail Highway as a continuous  
101 section of quartz arenite and shale forming slopes and moderately steep hillsides with limestone  
102 forming prominent ledges (Figs. 1 and 2). The Zabriskie Quartzite is dominated by burrowed and  
103 hummocky cross-bedded quartz arenite beds (Prave, 1991; Keller et al., 2012). It lacks age-diagnostic  
104 fossils, but rocks immediately above and below have yielded fauna from the *Bonnia-Olenellus*  
105 trilobite zone of Series 2 (Diehl, 1974; Palmer and Halley, 1979; Prave, 1991; Peng et al., 2012).

106           The Carrara Formation comprises cycles of silty marl and limestone with a trilobite fauna  
107 spanning the *Bonnia-Olenellus* to the *Glossopleura* zones, and thus the Series 2 - Series 3 boundary  
108 (Adams, 1995; Palmer and Halley, 1979; Sundberg and McCollum, 2000; Babcock et al., 2012; Keller  
109 et al., 2012; Fig. 3). The unit has been divided into nine members in the western Great Basin: Eagle  
110 Mountain Shale, Thimble Limestone, Echo Shale, Gold Ace Limestone, Pyramid Shale, Red Pass  
111 Limestone, Pahrump Hills Shale, Jangle Limestone and the Desert Range Limestone (Palmer and  
112 Halley, 1979). However, there is significant lateral variation within the Carrara Formation and at  
113 Emigrant Pass, the Thimble Limestone is not present (Palmer and Halley, 1979; Adams and  
114 Grotzinger, 1996). Overall the carbonate content of the Carrara Formation decreases in more  
115 basinward settings to the west (Hogan et al., 2011; Keller et al., 2012; Foster, 2014). Within the  
116 Carrara Formation at Emigrant Pass, five members are important to this study.

117           The Eagle Mountain Shale Member consists of green to grey-brown silty shale with  
118 interbedded lenses and beds of bioclastic limestone developed towards the top (Palmer and Halley,  
119 1979). This is overlain by the Echo Shale Member which consists of green, platy shale and brown-  
120 orange limestone. The Echo Shale is correlated with the basal Combined Metals Member of the  
121 Pioche Formation in eastern Nevada (Palmer and Halley, 1979). The succeeding Gold Ace Limestone  
122 is a prominent, cliff-forming limestone (Cornwall and Kleinhampl, 1961). The strata include thin to

123 medium-bedded lime mudstone, with dolomitic beds and oncolitic limestone (Palmer and Halley,  
124 1979). Based on shared trilobite zones, the Gold Ace Limestone correlates with the Combined  
125 Metals Member of the Pioche Formation at Oak Springs Summit (Merriam and Palmer, 1964).

126 The overlying Pyramid Shale Member is a green shale with interbeds of brown and maroon  
127 silty marl and lenses of oncolitic and bioclastic limestone. Trilobite biostratigraphy indicates the  
128 Pyramid Shale is equivalent to two members of the Pioche Formation in eastern Nevada: the C-Shale  
129 Member and the Susan Duster Limestone Member (Palmer and Halley, 1979; Palmer, 1998). The Red  
130 Pass Limestone Member is the youngest unit examined in Death Valley. It forms prominent cliffs of  
131 oncolitic and bioclastic limestone, laminated lime mudstone and fenestral lime mudstone (Palmer  
132 and Halley, 1979). There is no equivalent limestone unit in the Pioche Formation of Nevada (Palmer  
133 and Halley, 1979).

134

## 135 2.2. Oak Springs Summit

136 At Oak Springs Summit, the Pioche Formation crops out to the west of a parking area in a dry  
137 river bed. Limestone forms more prominent ledges and platforms whilst shale forms recessively  
138 weathered outcrop (Figs. 1 and 2). The Combined Metals Member is composed of silty, oncolite-  
139 bearing dark limestone with *Olenellus* (Palmer, 1998; Sundberg and McCollum, 2000; Hollingsworth  
140 et al., 2011). It is overlain by the C- Shale Member (formerly the Comet Shale), a series of shale and  
141 thin-bedded limestone beds with pinch-and-swell bed boundaries (Palmer, 1998; Sundberg and  
142 McCollum, 2000). The Series 2 - Series 3 boundary is placed at the base of the C-Shale due to the  
143 sudden disappearance of the Olenellidae, and their replacement by a fauna dominated by  
144 *Eoptychoparia piochensis* at this level (Palmer, 1998; Sundberg and McCollum, 2000). The  
145 succeeding Susan Duster Limestone Member is a well-bedded, grey marl with occasional argillaceous  
146 and bioclastic limestone beds composed of trilobite fragments (Merriam and Palmer, 1964).

147

### 148 2.3. Biostratigraphy

149 Trilobite assemblages from the Carrara and Pioche formations belong to the *Olenellus*,  
150 *Eokochaspis nodosa*, *Amecephalus arrosensis* and the *Plagiura-Poliella* zones that provide a  
151 framework for regional correlation (Merriam and Palmer, 1964; Palmer and Halley, 1979; Fig. 3). The  
152 *Olenellus* Zone ranges from the Zabriskie Quartzite to the basal portion of the Pyramid Shale  
153 Member within Death Valley (Palmer and Halley, 1979; Fig. 2). In Nevada, this zone spans the  
154 Delamar Member to the base of the C-Shale (Merriam and Palmer, 1964; Sundberg and McCollum,  
155 2000). All olenellid trilobites disappear over a ~ 2 cm interval at the top of the zone, forming a  
156 distinct extinction horizon (Palmer, 1998; Fig. 2). This is immediately followed by first appearance of  
157 the ptychopariid trilobite *Eokochaspis nodosa*, which defines both the base of the *E. nodosa* Zone,  
158 and the Series 2 - Series 3 boundary (Sundberg and McCollum, 2000; Fig. 2). *E. nodosa* Zone faunas  
159 also occur in the Pyramid Shale Member in Death Valley (Sundberg and McCollum, 2000).

160 The succeeding *Amocephalus arrosensis* Zone contains *A. arrosensis*, *Mexicella robusta*  
161 and *Kochina? walcotti*. The zone is best defined at Hidden Valley, Nevada, where its base is 30 m  
162 above the base of the C-Shale Member (Merriam and Palmer, 1964), but it has not been recorded in  
163 the Carrara Formation due to a paucity of fossils above the *E. nodosa* Zone in the Pyramid Shale  
164 (Palmer and Halley, 1979). However, trilobites, from the *Plagiura-Poliella* Zone, reappear in the  
165 uppermost Pyramid Shale and lower Red Pass Limestone (Palmer and Halley, 1979).

166

### 167 3. Methods

168 Sedimentary logging of the Carrara and Pioche formations was undertaken. At Emigrant  
169 Pass, 170 m of the Carrara Formation was logged from the base of the formation (at the contact with  
170 the Zabriskie Quartzite) up to the Red Pass Limestone Member. At Oak Springs Summit a 53 m-thick  
171 section of the Pioche Formation was logged, ranging from the basal Combined Metals Member to  
172 Susan Duster Limestone Member, an interval correlative with the Emigrant Pass section based on

173 trilobite biostratigraphy (Merriam and Palmer, 1964; Palmer and Halley, 1979; Fig. 2). From these  
174 logs, four facies were defined (discussed below, Table 1). At the two study sections, 30 samples from  
175 the Pioche Formation and 57 samples from the Carrara Formation were analysed for  $\delta^{13}\text{C}_{\text{carb}}$  (Table  
176 2). In Lincoln County, Nevada, we also sampled the Ruin Wash location (Palmer, 1998; Lieberman,  
177 2003) for additional facies and framboid analysis. Ruin Wash provided a second section (after Oak  
178 Springs Summit) where the extinction horizon of the olenellids is clearly seen (see Supplementary  
179 Material, Fig. S1). Facies analysis was undertaken in the field and complemented by petrographic  
180 examination of 49 thin sections. In order to evaluate redox conditions, pyrite framboid size  
181 distribution was also assessed on 21 samples using a scanning electron microscope (FEI Quanta 650  
182 FEG-ESEM) in backscatter mode (see Bond and Wignall (2010) for procedure).

183         The calcite carbon ( $^{13}\text{C} / ^{12}\text{C}$ ) and oxygen ( $^{18}\text{O} / ^{16}\text{O}$ ) isotope values of powdered bulk  
184 sediment samples were measured on a total of 98 samples at the GeoZentrum Nordbayern, FAU  
185 Erlangen-Nurnberg, Germany (27 samples) and the School of Environmental Sciences, University of  
186 Liverpool, UK (71 samples). Carbon dioxide was prepared by reaction with phosphoric acid either at  
187 70°C using a Gasbench II preparation system (FAU) or at 25 °C using the classical, ‘sealed vessel’  
188 method (UoL). Mass ratios of the resultant purified gases were measured with a ThermoFisher Delta  
189 V plus mass spectrometer operating in continuous flow mode (FAU) or a VG SIRA 10 dual-inlet mass  
190 spectrometer (UoL). Raw gas data were corrected for  $^{17}\text{O}$  effects and calibrated to the VPDB scale  
191 using a combination of international reference materials ( $\delta^{13}\text{C}$  values are assigned as +1.95 ‰ to  
192 NBS 19 and -46.6 ‰ to LSVEC and  $\delta^{18}\text{O}$  values of -2.20 ‰ to NBS19 and -23.2 ‰ to NBS18) and  
193 laboratory quality control materials and reported as conventional delta ( $\delta$ ) values. Analytical  
194 precision ( $1 \sigma$ ) is estimated to be better than 0.1 ‰ for both isotope ratios based on replicate  
195 analysis of standards. Some notable differences in oxygen isotope values were reported where  
196 specific samples were duplicated by both laboratories. The reason for these differences is uncertain.  
197 Although some discrepancies were found to be significant, they do not impact on either the  
198 palaeoenvironmental or chemostratigraphic interpretation of the carbon isotope data.

199 The topmost 8 samples of the Carrara Formation were analysed at the University of  
200 Massachusetts, Amherst. Powdered, homogenized samples were analysed for  $\delta^{13}\text{C}_{\text{carb}}$  and  $\delta^{18}\text{O}_{\text{carb}}$   
201 values using a Finnigan Delta XL+ isotope ratio mass spectrometer with an automated carbonate  
202 prep system (Kiel III). We report results as the per mille difference between sample and the VPDB  
203 standard in delta notation where  $\delta^{18}\text{O}$  or  $\delta^{13}\text{C} = (R_{\text{sample}} / R_{\text{standard}} - 1) \times 1000$ , and R is the ratio of the  
204 minor to the major isotope. Results were calibrated using a house standard (crushed, washed and  
205 sieved marble) with VPDB values of +1.28 for  $\delta^{13}\text{C}$  ‰ and -8.48 ‰ for  $\delta^{18}\text{O}$ . Reproducibility of  
206 standard materials is 0.1 ‰ for  $\delta^{18}\text{O}$  and 0.05 ‰ for  $\delta^{13}\text{C}$ .

207 Total carbon (TC) and total organic carbon (TOC), following removal of calcite by acid  
208 decomposition of bulk sediment samples, was measured using a LECO SC-144DR Dual Range carbon  
209 and sulphur analyser at the University of Leeds. Total inorganic carbon (TIC) was subsequently  
210 calculated by difference (TIC = TC - TOC). An estimate of the calcite content for each sample was  
211 made by assuming that all TIC is hosted by calcite (wt % calcite = TIC x 8.333).

212

## 213 **4. Results**

### 214 *4.1. Facies Analysis*

215 Four facies and nine sub-facies were identified (Table 1): grainstone, packstone, silty marl  
216 and marl and they have been grouped into an onshore-offshore trend spanning shallow subtidal to  
217 outer shelf environments (Table 1). The shallowest strata consist of grainstone facies with common  
218 shell hash that is often abraded. Beds are typically decimetres thick and can show a hummocky top  
219 surface and sharp, erosive bases. Inclined stacks of flat-pebble intraclasts with herringbone-like cross  
220 stratification are present, suggesting storm wave processes (Fig. 4D). Bioturbated packstone, with  
221 sub-facies of oncolitic, bioclastic and silty packstone varieties (Fig. 5B), are interpreted to be a  
222 deeper facies based on the presence of a micritic mud matrix. Deeper water silty marl include fissile,  
223 homogenous and thoroughly bioturbated variants. Deepest-water, most offshore successions are

224 dominated by fine grained marl, including sub-facies of laminated, pyritic dolomicrite and  
225 bioturbated marl with ichnofabric index (II) values of 2 - 3 (II2 and II3) in the scheme of Droser and  
226 Bottjer (1986).

227 The facies distribution reveals consistent trends in the two principal study sections. The base of  
228 the Carrara Formation, seen at Emigrant Pass, is dominated by deeper water facies (Facies 4) of the  
229 Eagle Mountain Shale. Commonly, the marl has a grey-green colour produced by the abundance of  
230 chlorite and clinocllore in the matrix (Figs. 4F, 5A and 6E). Laminated intervals are common,  
231 although these occur interbedded with burrowed strata suggesting there were frequent fluctuations  
232 of redox conditions.

233 The exception to the generally quiet, low-energy deposition of the Eagle Mountain Shale is  
234 recorded by a sharp, erosive-based bed of Facies 1 developed just over 30 m above the base of the  
235 section. This shelly, oncolitic packstone contains rip-up clasts of the underlying marl and sole marks  
236 on its base (Fig. 7A). Internally, thin intraclasts and shells display a chevron-stacking pattern (Fig.  
237 4D). A major storm event seems likely to have produced this horizon with the shell-stacking  
238 produced by powerful bi-directional currents. The succeeding Echo Shale and Gold Ace members  
239 record shallowing. Grainstone and packstone dominate this 20-m-thick interval which includes  
240 erosive-based oncolitic packstone beds (Fig. 7B). Above this in the Pyramid Shale Member marl  
241 facies dominate, taken to be indicative of a sustained deepening. Grainstone and packstone facies  
242 developed in the lower ~ 15 m of the member are interpreted to have been transported during  
243 storm events. It is within this transgressive phase that the Series 2 - Series 3 boundary is recorded,  
244 along with the olenellid extinction (Foster, 2014). Deep-water sedimentation is abruptly terminated  
245 by the development of shallow-water grainstone at the base of the Red Pass Limestone Member  
246 (Fig. 7). Ooids and abraded fossil material (Table 1, Sub-Facies 1.1) suggest a nearshore setting.

247 The Pioche Formation at Oak Springs Summit records a more distal version of the succession  
248 seen within the Carrara Formation with relatively deep-water Facies 3 and 4 dominating (Fig. 2),

249 though the same overall deepening-upwards trend is seen. Thus, the lower half of the Combined  
250 Metals Member consists of alternating silty marl and packstone. Above this, the remainder of the  
251 section is dominated by deeper-water facies (Fig. 2). The uppermost Combined Metals Member and  
252 the majority of the C-Shale Member record a similar transgressive deepening seen within the  
253 Pyramid Shale Member of the Carrara Formation. The olenellid extinction level occurs within this  
254 transgressive succession between a marl and a silty marl in the base of the C-Shale Member (Fig. 4E).  
255 This minor facies shift does not represent a significantly different environment and as such  
256 extinction is not thought to be a function of facies change. Immediately above the extinction  
257 horizon, chlorite in the form of both rounded grains and cement becomes common (Fig. 5A). The  
258 remainder of the C-Shale Member is a thick package of marl that transitions to silty marl at the base  
259 of the Susan Duster Limestone.

260

#### 261 4.2. Pyrite Framboid Analysis

262 Framboid size analysis was performed on the Series 2 - Series 3 boundary strata (and thus  
263 the extinction horizon) from the Pioche Formation at Oak Springs Summit, where 11 samples were  
264 collected in a 7 m interval spanning 3.5 m either side of the extinction horizon. All samples contained  
265 abundant scattered crystals of pyrite ranging in size from 1-10  $\mu\text{m}$ , often found agglomerated in  
266 clustered patches. Five samples yielded framboids preserved as iron oxyhydroxides due to  
267 weathering, with only minor amounts of original pyrite preserved in their core. The framboids  
268 showed a size distribution spanning an anoxic-dysoxic range (Fig. 8). The most dysoxic sample  
269 (smallest mean framboid diameter size and size range, lowest standard deviation) occurred in a marl  
270 approximately 1 m below the extinction horizon. Dysoxic framboid populations also occurred in the  
271 1 m of strata overlying the extinction level. However, a sample from 20 cm below the extinction  
272 level did not yield any pyrite framboids suggesting fully oxygenated conditions. This variable degree

273 of oxygen-restriction suggested by the framboid analysis is also seen in the variability of the  
274 associated sedimentary fabrics, which varies from laminated to slightly burrowed (II2).

275           Seven samples were also analysed from the Pioche Formation at Ruin Wash where the  
276 olenellid extinction horizon has been located within a succession of marls (Palmer, 1998; Lieberman,  
277 2003; Fig. S1). Generally, framboidal pyrite was absent at this location with the exception of two  
278 samples from 10 and 15 cm below the extinction horizon where they had size ranges that plot in the  
279 anoxic field (Fig. 8). An additional four samples from around the extinction horizon at Emigrant Pass  
280 were also analysed. In this case, all samples only yielded scattered pyrite crystals but not framboids,  
281 suggesting better oxygenated conditions in this shallower-water section.

282

### 283 4.3. Chemostratigraphy

284           In the basal 20 m of the Carrara Formation  $\delta^{13}\text{C}$  values are highly variable and do not show a  
285 clear trend (Fig. 7), but they then begin to stabilise around  $-2\text{‰}$  before a consistent positive trend  
286 develops. In the Pyramid Shale Member the base of the negative excursion begins with at  $-0.1\text{‰}$ ,  
287 above this  $\delta^{13}\text{C}_{\text{carb}}$  values begin a decline to a lowpoint at 105 m of  $-3.5\text{‰}$  (a negative shift of 3.4  
288  $\text{‰}$ ). In the overlying 25 m, no data was obtained because carbonate values were too low for  
289 analysis. Above this gap,  $\delta^{13}\text{C}_{\text{carb}}$  values show a positive trend, returning to values around  $-0.1\text{‰}$ ,  
290 similar to those from the base of the section.

291           Barring one outlier at the base of the section,  $\delta^{13}\text{C}_{\text{carb}}$  values from the first 13 m of the  
292 Pioche Formation remain around  $-2.5\text{‰}$  before there is a sharp, positive shift to  $-1.0\text{‰}$  over the  
293 next 15 m (Fig. 7). From this value of  $-1.0\text{‰}$  a negative shift occurs, resulting in peak negative  
294 values of  $-4.8\text{‰}$ . The nadir at the base of the C-Shale Member marks an overall shift of  $-3.8\text{‰}$ , a  
295 similar size to that found at Emigrant Pass. At the top of the section values return to around  $0\text{‰}$ .

296

## 297 5. Discussion

### 298 5.1. Carbon isotopes and diagenesis

299 In order to evaluate the reliability of our isotope data we assess the preservation of a  
300 primary carbon isotope signal in our samples. In both the Carrara and Pioche formations the isotope  
301 analyses are derived from samples with a wide range of carbonate values (Table 2). The high TIC  
302 samples are likely to record primary carbon isotope signatures since they are buffered from external  
303 change by a large carbonate-carbon reservoir (Saltzman and Thomas, 2012). Lower TIC samples are  
304 more susceptible to post depositional isotopic alteration or addition of carbonate with a non-  
305 primary carbon isotope composition (Brand and Veizer, 1981; Banner and Hanson, 1990; Marshall,  
306 1992). In both sections, the excursion to the lowest  $\delta^{13}\text{C}_{\text{carb}}$  values occurs at the level of the trilobite  
307 extinction (mid-Pyramid Shale, Carrara Formation and basal C-Shale, Pioche Formation) where TIC is  
308  $< 2$  wt. %. Here we assess the preservation of a primary carbon isotope composition, particularly in  
309 samples with low TIC.

310 Two diagenetic processes can alter the primary isotopic composition: recrystallization of  
311 carbonate or precipitation of additional authigenic carbonate with a distinct isotope composition  
312 (Marshall, 1992). Both marine pore fluids and meteoric waters can have dissolved inorganic carbon  
313 (DIC) enriched in  $^{12}\text{C}$  from the oxidation of organic matter and these mechanisms have differing  
314 predictions of the  $\delta^{13}\text{C}_{\text{carb}}$  and  $\delta^{18}\text{O}_{\text{carb}}$  values preserved (Marshall, 1992). Both the Carrara and  
315 Pioche formations display commonalities in their relationships between their  $\delta^{13}\text{C}_{\text{carb}}$  and  $\delta^{18}\text{O}_{\text{carb}}$   
316 ratios and their TIC and TOC concentrations. Firstly (point 1), neither formation shows a clear  
317 relationship between  $\delta^{13}\text{C}_{\text{carb}}$  and  $\delta^{18}\text{O}_{\text{carb}}$  (Figs. S2 and S3). Secondly (point 2), samples with the most  
318 negative  $\delta^{13}\text{C}_{\text{carb}}$  and the most positive  $\delta^{18}\text{O}_{\text{carb}}$  are mostly characterised by low TIC (defined as  $< 2$   
319 wt. %). Both the Carrara and Pioche formations exhibit generally low TOC (point 3). In the Carrara  
320 Formation TOC concentrations range from 5.17 to 0.0 wt. % TOC with a mean concentration of 0.14  
321 wt. % TOC. In the Pioche Formation concentrations range from 2.69 to 0.0 wt. % TOC, with a mean of

322 0.12 wt. % TOC. Finally (point 4), high TOC samples are characterised by more positive  $\delta^{13}\text{C}_{\text{carb}}$ . The  
323 major difference between the sections for these parameters is a much clearer positive relationship  
324 between TIC and  $\delta^{13}\text{C}_{\text{carb}}$  within the Pioche Formation.

325         These observations rule out wholesale recrystallization in a meteoric fluid since neither  
326 section displays a positive correlation between  $\delta^{18}\text{O}_{\text{carb}}$  and  $\delta^{13}\text{C}_{\text{carb}}$  (point 1, Figs. S2 and S3). The  
327 generally low TOC concentrations and the relationship between TOC and  $\delta^{13}\text{C}_{\text{carb}}$  (point 3 and 4) also  
328 makes localised precipitation of organic-carbon derived DIC doubtful. From the relationships  
329 between  $\delta^{18}\text{O}_{\text{carb}}$  and TIC (point 2) it is likely that a proportion of the low TIC samples (< 2 wt. %)  
330 have undergone variable resetting of their  $\delta^{18}\text{O}_{\text{carb}}$  towards more positive values. This observation is  
331 not consistent with precipitation of additional carbonate from unmodified meteoric or marine early  
332 diagenetic pore fluids, where the expectation would be a change towards more negative  $\delta^{18}\text{O}_{\text{carb}}$   
333 values (Marshall, 1992; Knauth and Kennedy, 2009; Cochran et al., 2010; Saltzman and Thomas,  
334 2012). The remaining possibility to explain the oxygen isotope relationships is variable exchange  
335 with, or precipitation of carbonate from, a hypothetical high  $\delta^{18}\text{O}$  fluid (Glumac and Walker, 1998).  
336 Since the climate at both sites is currently arid, one possibility is that the fluid in question is derived  
337 from evaporated modern meteoric water, but other possibilities exist (Saltzman and Thomas, 2012).

338         The relationships between  $\delta^{13}\text{C}_{\text{carb}}$  and TIC differ somewhat from those between  $\delta^{18}\text{O}_{\text{carb}}$  and  
339 TIC: from the Carrara Formation, the range of  $\delta^{13}\text{C}_{\text{carb}}$  in the < 2 wt. % TIC samples overlaps strongly  
340 with the range found in near pure limestone samples suggesting that the influence of diagenetic  
341 process on  $\delta^{13}\text{C}_{\text{carb}}$  at this site is likely to be minimal (Fig. S4). In contrast, samples from the Pioche  
342 Formation display a much clearer division between these two groups (TIC groups annotated in Fig.  
343 S5). This suggests that the influence of post-depositional process on  $\delta^{13}\text{C}_{\text{carb}}$  may have been more  
344 pronounced at this site. However, the  $\delta^{18}\text{O}_{\text{carb}}$  ranges of both high and low TIC samples of the Pioche  
345 Formation overlap (Fig. S6), indicating that at least some of the carbon isotope values have  
346 undergone minimal resetting.

347 In summary, there is clear evidence for a variable degree of oxygen isotope resetting  
348 towards more positive values, which is particularly pronounced in samples with low TIC (< 2 wt. %).  
349 There is also some evidence of concurrent variable resetting of carbon isotopes to more negative  
350 values in low TIC samples, with this being somewhat more pronounced in the Pioche Formation.  
351 Nonetheless, the presence of the negative  $\delta^{13}\text{C}_{\text{carb}}$  values and the consistency of the magnitude of  
352 the excursion at level of the Series 2 - Series 3 boundary (e.g., Zhu et al., 2006; Faggetter et al.,  
353 2016), correlated independently by biostratigraphy between the two sections suggest that these  
354 samples record a predominantly primary signal. As such, we conclude that the negative  $\delta^{13}\text{C}_{\text{carb}}$   
355 excursion within the Carrara and Pioche formations preserves a primary record, given its co-  
356 occurrence with the olenellid extinction horizon, we interpret it to be ROECE.

357

## 358 *5.2. Extinction and palaeoenvironmental change*

359 Identification of the ROECE in the Pioche and Carrara formations (Fig. 7) confirms the close  
360 temporal relationship between trilobite extinctions and carbon isotope excursions (Zhu et al., 2006;  
361 Faggetter et al., 2016). It also allows examination of the associated facies and relative sea-level  
362 changes at this time. Initially the Sauk I/II supersequence boundary was placed around the Series 2 -  
363 Series 3 boundary (Sloss 1963). However, more recently this has been placed lower in the succession  
364 at the top of the Zabriskie Quartzite, underlying the Carrara Formation (Prave, 1991). Thus the  
365 Carrara Formation falls entirely within Sauk II (Keller et al., 2003, 2012; Morgan, 2012). Nonetheless,  
366 there are alternative regression surfaces in the Carrara Formation. A candidate for a sequence  
367 boundary occurs at the base of the Red Pass Limestone where there is a sharp transition from deep-  
368 water to shallow-water. This level lies around 45 m above ROECE in the Carrara Formation.

369 Rather than regression, the olenellid extinction occurs within a deepening succession.  
370 Transgression and shelf anoxia often go hand-in-hand, and oxygen stress has been implicated in  
371 ROECE extinction (Montañez et al., 2000). However, at Oak Springs Summit, pyrite framboid analysis

372 suggests dysoxic but not euxinic conditions in the extinction interval, and the shallower study  
373 locations show no evidence for oxygen restriction. The evidence for intensified oxygen-restricted  
374 deposition at the trilobite extinction level is therefore weak. It also noteworthy that low-oxygen  
375 conditions were common in Cambrian oceans (Hurtgen et al., 2009; Pruss et al., 2010; Gill et al.,  
376 2011), and there is no suggestion that anoxia was intensified at the level of ROECE.

377         The Series 2 - Series 3 boundary interval saw the eruption of the Kalkarindji flood basalt  
378 province (Glass and Phillips, 2006; Jourdan et al., 2014; Marshall et al., 2016). In younger intervals of  
379 the Phanerozoic, the formation of large igneous provinces frequently coincides with mass  
380 extinctions (Wignall, 2015; Bond and Grasby, 2016) and the eruption of large volumes of volcanic  
381 volatiles provides a causal mechanism for driving biologic crises. The contemporaneous negative  
382  $\delta^{13}\text{C}$  signal of ROECE is often seen at times of LIP eruptions and may record the influx of isotopically-  
383 light volcanic  $\text{CO}_2$  (e.g., Payne et al. 2004). Thus, in many regards the ROECE has the hallmarks of  
384 later Phanerozoic LIP-related mass extinctions although evidence for the commonly associated  
385 environmental changes such as the spread of anoxia (Wignall, 2015), is not clearly established for  
386 this Cambrian example.

387

## 388 **6. Conclusions**

389         In the western Great Basin, USA, the extinction of the dominant olenellid trilobites occurs  
390 within a deepening-upward shelf succession. A major  $-3.5\%$  negative carbon isotope excursion  
391 (ROECE) occurs at the same level. This extinction/isotope event occurs around the Cambrian Series 2  
392 - Series 3 boundary interval. Pyrite framboid size distribution data and laminated facies suggest  
393 periodic dysoxia occurred in the facies immediately surrounding the extinction horizon. However,  
394 these conditions were neither widespread (shallower-water boundary sections in Death Valley do  
395 not record oxygen starvation) nor especially unusual (laminated strata are sporadically developed  
396 throughout the offshore units of the Carrara Formation) suggesting dysoxia did not play a major role

397 in the extinction. The environmental effects of the contemporaneous Kalkarindji flood basalt  
398 province of Australia provide a better potential causal for the extinction at the Series 2 - Series 3  
399 boundary, although detailed correlation with the sections in North America is required.

400

#### 401 **Acknowledgments**

402 We thank Emily Smith, Kristin Bergmann, and Jessica Creveling for valuable discussions in the field.

403 We also thank Tessa Browne, along with Helena Tatgenhorst for allowing the use of their C isotope

404 data in the top 25 m of Emigrant Pass, and Stephen Burns in the stable isotope laboratory at the

405 University of Massachusetts at Amherst for providing these carbon isotope analyses. We thank an

406 anonymous reviewer for their constructive feedback, and Jessica Creveling for her extensive and

407 thorough review. This research was funded by a NERC postgraduate studentship to LEF.

408

#### 409 **Figure captions**

410 Figure 1. Location map showing study sections at Emigrant Pass, Death Valley region, California (35°

411 53' 29.24"N, 116° 04' 39.08"W) and Oak Springs Summit, Burnt Spring Range, Lincoln County,

412 Nevada (37°37'04.32"N 114°43'17.20"W). Star indicates approximate location of field area during

413 the Cambrian Series 2 (after McKerrow et al., 1992).

414 Figure 2. Biostratigraphic correlation of the trilobite zones of the Carrara and Pioche formations

415 (Palmer and Halley, 1979; Sundberg and McCollum, 2000). Facies column is based on field and

416 petrographic observations, and numbers relate to facies detailed in Table 1. A generalised

417 stratigraphic column of Precambrian and Cambrian formations in Death Valley is given (from Corsetti

418 and Hagadorn, 2000).

419 Figure 3. Correlation of trilobite biozones within the Carrara and Pioche formations (Merriam and

420 Palmer, 1965; Palmer and Halley, 1979; Sundberg and McCollum, 2000). *O.* is *Olenellus*, *P.* is *Poliella*.

421 Figure 4. Field photographs.

422 A. Trilobite debris (spines and carapaces and hyoliths) in a bioclastic hash on bedding planes of  
423 oolitic grainstone, Carrara Formation. B. Oncolitic packstone facies at Emigrant Pass. C. Bifurcating  
424 burrows in well bioturbated silty marl at Emigrant Pass, notebook for scale. D. Oolitic grainstone  
425 facies showing inclined chevron-style packing of thin intraclast and bioclasts (hyolith, ooid and other  
426 detrital fragments). E. Olenellid extinction level at the base of the C-Shale Member at Oak Springs  
427 Summit. Red line indicates extinction horizon from Palmer (1998). F. Fissile, laminated marl and silty  
428 marl in the lower Eagle Mountain Shale at Emigrant Pass. G. *Thalassinoides* in fine-grained, silty marl  
429 of the Carrara Formation. H. Vertical burrows (at the hammer tip) in silty marl beds of the Carrara  
430 Formation.

431 Figure 5. Scans of thin sections and photomicrographs.

432 A. Photomicrograph of a range of chlorite in the silty marl facies immediately above the extinction  
433 horizon at Oak Springs Summit. Chlorite occurs as elongate grains and also as cement. B:  
434 Photomicrograph of a silty bioclastic packstone in the upper Eagle Mountain Shale. C: Scan of slide of  
435 oncolitic packstone (Eagle Mountain Shale) showing oncoids with bioclastic nucleus of echinoderm  
436 plates amongst a matrix of shell detritus and micrite. D: Scan of slide of bioclastic grainstone.  
437 Elongate, trilobite fragments dominate this facies alongside hyolith remains and echinoderm plates.  
438 Dark brown mineral growth shows iron oxide preferentially replacing shell material.

439 Figure 6. Scans of thin sections and photomicrographs.

440 A: Scan of silty marl showing quartz grains and detrital chlorite grains (green). B: Photomicrograph of  
441 marl facies in the Combined Metals Member, Pioche Formation. Trilobite carapace exhibits brown  
442 needle like iron oxide replacement of the calcite shell. C: Photomicrograph of peloidal grainstone  
443 facies in the Combined Metals Member, Pioche Formation. Well rounded micrite pellets alongside  
444 rounded quartz grains amongst a fine micrite matrix. D: Photomicrograph of oolitic, bioclastic  
445 grainstone with iron oxides partially replacing ooids. E: Photomicrograph of silty chloritic limestone

446 showing rounded chlorite grains (white dashed lines). F: Photomicrograph of chloritic silty marl  
447 facies showing sub-angular to angular quartz sand grains alongside hololith and trilobite debris.

448 Figure 7. Carbon isotope chemostratigraphy of the Carrara Formation at Emigrant Pass and Pioche  
449 Formation at Oak Springs Summit. A. Inset log shows contact between silty micrite and an erosive-  
450 based oncolitic packstone with rip up clasts of the underlying silty micrite. This horizon grades  
451 laterally into an oolitic grainstone. B. Inset log of contact between silty bioclastic packstone and an  
452 erosive-based oncolitic packstone. Both erosional surfaces mark the transport of shallow water  
453 bioclastic material during storm events.

454 Figure 8. Size versus standard deviation for framboids from Series 2 - Series 3 boundary strata of  
455 California and Nevada showing the presence of oxygen-restricted facies. The threshold separating  
456 euxinic/anoxic and dysoxic/oxic size ranges in modern environments is from Wilkin et al. (1996).

457 Table 1: Facies of the Carrara and Pioche formations.

458 Table 2. Geochemical and framboid measurements for the Carrara and Pioche formations at  
459 Emigrant Pass (EP) and Oak Springs Summit (OSS) and framboid data from the Pioche Formation at  
460 Ruin Wash (RW).

461

## 462 References

463 Adams, R. D. (1995). Sequence-stratigraphy of Early-Middle Cambrian grand cycles in the Carrara  
464 Formation, southwest Basin and Range, California and Nevada. In *Sequence Stratigraphy and*  
465 *Depositional Response to Eustatic, Tectonic and Climatic Forcing* (pp. 277-328). Springer  
466 Netherlands.

467 Adams, R.D., Grotzinger, J. P. (1996). Lateral continuity of facies and parasequences in Middle  
468 Cambrian platform carbonates, Carrara Formation, southeastern California, USA. *Journal of*  
469 *Sedimentary Resesearch*, 66(6), 1079-1090.

- 470 Banner, J.L., Hanson, G. N. (1990). Calculation of simultaneous isotopic and trace element variations  
471 during water-rock interaction with applications to carbonate diagenesis. *Geochim. Cosmo.*  
472 *Acta* 54(11), 3123-3137.
- 473 Bond, D.P.G., Grasby, S.E. (2016). On the causes of mass extinctions. *Palaeogeography,*  
474 *Palaeoclimatology, Palaeoecology. (In this issue).*
- 475 Bond, D.P.G, Wignall, P.B. (2010). Pyrite framboid study of marine Permian-Triassic boundary  
476 sections: a complex anoxic event and its relationship to contemporaneous mass  
477 extinction. *Geological Society of America Bulletin*, 122(7-8), 1265-1279.
- 478 Bond, G. C., and Kominz, M. A. (1984). Construction of tectonic subsidence curves for the early  
479 Paleozoic miogeocline, southern Canadian Rocky Mountains: Implications for subsidence  
480 mechanisms, age of breakup, and crustal thinning. *Geological Society of America Bulletin*, 95(2),  
481 155-173.
- 482 Boucot, A. J. (1990). Phanerozoic extinctions: How similar are they to each other? In *Extinction*  
483 *Events in Earth History* (pp. 5-30). Springer Berlin Heidelberg.
- 484 Brand, U., Veizer, J. (1981). Chemical diagenesis of a multicomponent carbonate system-2: stable  
485 isotopes. *Journal of Sedimentary Petrology*, 51(3), 987-997.
- 486 Cochran, J. K., Kallenberg, K., Landman, N. H., Harries, P. J., Weinreb, D., Turekian, K. K., Cobban, W.  
487 A. (2010). Effect of diagenesis on the Sr, O, and C isotope composition of late Cretaceous  
488 mollusks from the Western Interior Seaway of North America. *American Journal of*  
489 *Science*, 310(2), 69-88.
- 490 Cornwall, H. R., Kleinhampl, F. J. (1961). Geology of the Bare Mountain Quadrangle, Nevada. USGS  
491 Report No. 157.
- 492 Corsetti, F. A., and Hagadorn, J. W. (2000). Precambrian-Cambrian transition: Death Valley, United  
493 States. *Geology*, 28(4), 299-302.

- 494 Debrenne, F. (1991). Extinction of the Archaeocyatha. *Historical Biology*, 5 (2-4), 95-106.
- 495 Diehl, P. E. (1974). Stratigraphy and sedimentology of the Wood Canyon Formation, Death Valley  
496 area, California. *Death Valley Region, California and Nevada, Geol Soc Am, Cordilleran Section*  
497 *Annual Meeting, 70<sup>th</sup>, Las Vegas, Nevada, 1974, Guidebook*, p. 37-48.
- 498 Droser, M.L., Bottjer, D.J. (1986). A semiquantitative field classification of ichnofabric: research  
499 method paper. *Journal of Sedimentary Research*, 56(4), 558-559.
- 500 Erdtmann, B.D., Miller, J.F. (1981). Eustatic control of lithofacies and biofacies changes near the base  
501 of the Tremadocian. In *Short Papers for the Second International Symposium on the Cambrian*  
502 *System. USGS Open-File Report*, 81-743, 78-81.
- 503 Faggetter, LE., Wignall, P.B., Pruss, S.B., Sun, Y., Raine, R.J., Newton, R.J., Widdowson, M.,  
504 Joachimski, M.M., Smith, P.M. (2016). Sequence stratigraphy, chemostratigraphy and facies  
505 analysis of Cambrian Series 2 - Series 3 boundary strata in northwest Scotland. *Geological*  
506 *Magazine*, pp. 1-13
- 507 Fan, R., Deng, S., Zhang, X. (2011). Significant carbon isotope excursions in the Cambrian and their  
508 implications for global correlations. *Science China Earth Sciences*, 54(11), 1686-1695.
- 509 Fedo, C.M., Cooper, J.D. (2001). Sedimentology and sequence stratigraphy of Neoproterozoic and  
510 Cambrian units across a craton-margin hinge zone, southeastern California, and implications for  
511 the early evolution of the Cordilleran margin. *Sedimentary Geology*, 141, 501-522.
- 512 Foster, J. (2014). *Cambrian ocean world: ancient sea life of North America*. Indiana University Press,  
513 432 pp.
- 514 Gill, B.C., Lyons, T.W., Young, S.A., Kump, L.R., Knoll, A.H., Saltzman, M.R. (2011). Geochemical  
515 evidence for widespread euxinia in the Later Cambrian ocean. *Nature*, 469(7328), 80-83.

- 516 Glass, L.M., Phillips, D. (2006). The Kalkarindji continental flood basalt province: a new Cambrian  
517 large igneous province in Australia with possible links to faunal extinctions. *Geology*, 34(6), 461-  
518 464.
- 519 Glumac, B., Walker, K.R. (1998). A Late Cambrian positive carbon-isotope excursion in the southern  
520 Appalachians: Relation to biostratigraphy, sequence stratigraphy, environments of deposition,  
521 and diagenesis. *Journal of Sedimentary Research*, 68(6), 1212-1222
- 522 Hallam, A., Wignall, P.B. (1997). *Mass extinctions and their aftermath*. Oxford University Press,  
523 Oxford, 320pp.
- 524 Hollingsworth, J.S., Sundberg, F.A., Foster, J.R. (2011). Cambrian stratigraphy and paleontology of  
525 Northern Arizona and Southern Nevada. *Museum of Northern Arizona Bulletin*, 67, 321.
- 526 Hogan, E.G., Fedo, C.M., Cooper, J.D. (2011). Reassessment of the basal Sauk Supersequence  
527 boundary across the Laurentian craton-margin hinge zone, southeastern California. *The Journal*  
528 *of Geology*, 119(6), 661-685.
- 529 Howley, R.A., Rees, M. N., Jiang, G. (2006). Significance of Middle Cambrian mixed carbonate-  
530 siliciclastic units for global correlation: southern Nevada, USA. *Palaeoworld*, 15(3), 360-366.
- 531 Hurtgen, M.T., Pruss, S. B., Knoll, A. H. (2009). Evaluating the relationship between the carbon and  
532 sulfur cycles in the later Cambrian ocean: an example from the Port au Port Group, western  
533 Newfoundland, Canada. *Earth and Planetary Science Letters*, 281(3), 288-297.
- 534 Jourdan, F., Hodges, K., Sell, B., Schaltegger, U., Wingate, M.T. D., Evins, L.Z., Blenkinsop, T. (2014).  
535 High-precision dating of the Kalkarindji large igneous province, Australia, and synchrony with  
536 the Early-Middle Cambrian (Stage 4-5) extinction. *Geology*, 42(6), 543-546.
- 537 Keller, M., Cooper, J., Lehnert, O. (2003). Sauk sequence sequences (southern Great Basin)  
538 [abstract]. In: Geological Society of American *Abstracts with Programs*, Vol. 35, No.6,  
539 September 2003, p.543

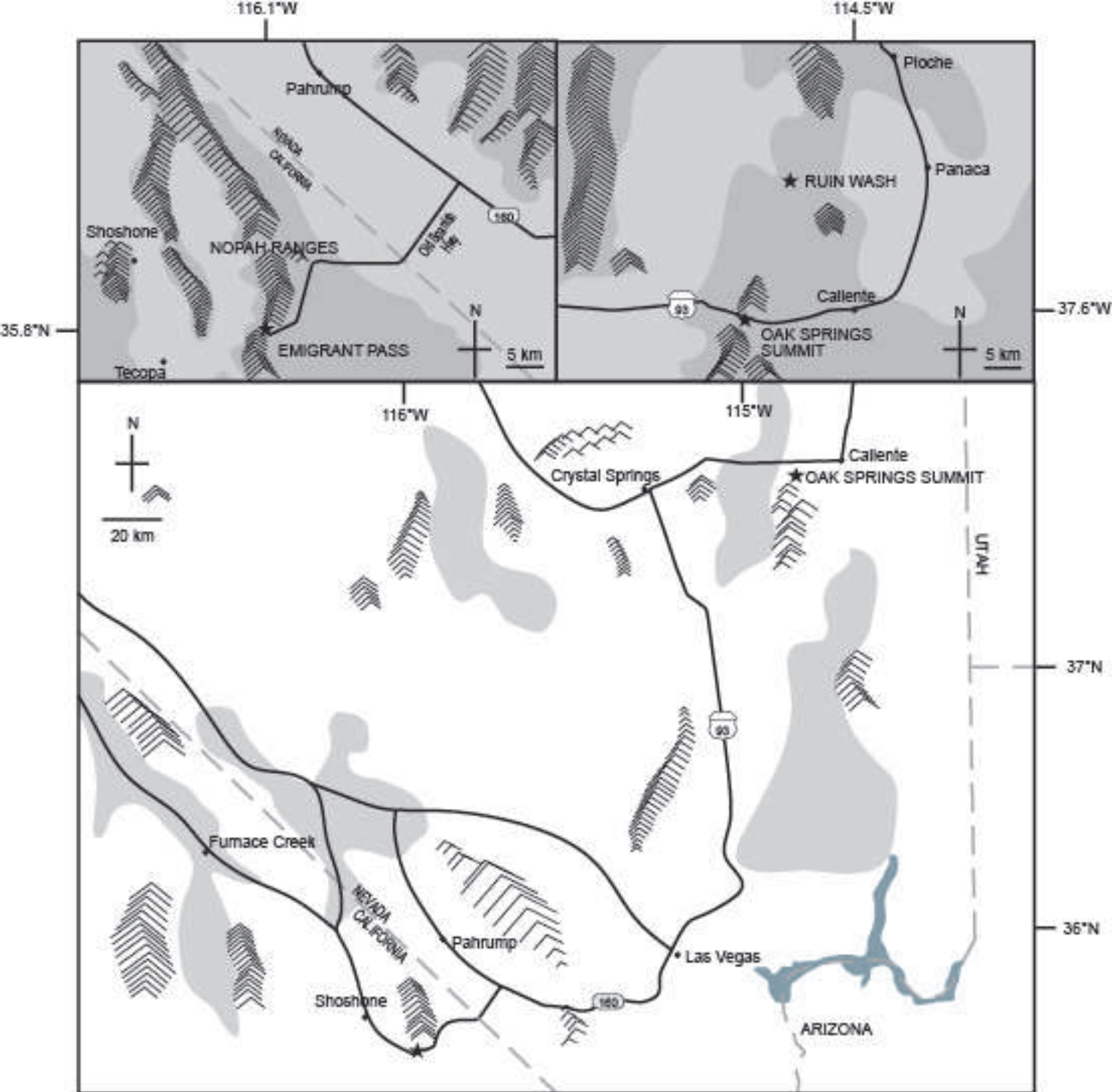
- 540 Keller, M., Cooper, J.D., Lehnert, O. (2012). Sauk megasequence supersequences, southern Great  
541 Basin: Second-order accommodation events on the southwestern Cordilleran margin platform,  
542 in J.R. Derby, R.D. Fritz, S.A. Longacre, W.A. Morgan, and C.A. Sternbach, eds., *The great*  
543 *American carbonate bank: The geology and economic resources of the Cambrian- Ordovician*  
544 *Sauk megasequence of Laurentia*: AAPG Memoir 98, p. 873- 896
- 545 Knauth, L.P., Kennedy, M.J. (2009). The late Precambrian greening of the Earth. *Nature*, 460(7256),  
546 728-732.
- 547 Landing, Ed, (2012). The great American carbonate bank in eastern Laurentia: Its births, deaths, and  
548 linkage to paleoceanic oxygenation (Early Cambrian - Late Ordovician), in J. R. Derby, R. D.  
549 Fritz, S. A. Longacre, W. A. Morgan, and C. A. Sternbach, eds., *The great American carbonate*  
550 *bank: The geology and economic resources of the Cambrian - Ordovician Sauk megasequence of*  
551 *Laurentia*: AAPG Memoir 98, p. 451 - 492.
- 552 Levy, M., Christie-Blick, N. (1991). Tectonic subsidence of the early Paleozoic passive continental  
553 margin in eastern California and southern Nevada. *Geological Society of America*  
554 *Bulletin*, 103(12), 1590-1606.
- 555 Lieberman, B.S. (2003). A new soft-bodied fauna: the Pioche Formation of Nevada. *Journal of*  
556 *Paleontology*, 77(04), 674-690.
- 557 MacNiocaill, C., Smethurst, M.A. (1994). Palaeozoic palaeogeography of Laurentia and its margins: a  
558 reassessment of palaeomagnetic data. *Geophysical Journal International*, 116(3), 715-725.
- 559 Marshall, J.D. (1992). Climatic and oceanographic isotopic signals from the carbonate rock record  
560 and their preservation. *Geological magazine*, 129(02), 143-160.
- 561 Marshall, P.E., Widdowson, M., Murphy, D. T. (2016). The giant lavas of Kalkarindji: rubbly pāhoehoe  
562 lava in an ancient continental flood basalt province. *Palaeogeography, Palaeoclimatology,*  
563 *Palaeoecology*, 441, 22-37.

- 564 McKerrow, W.S., Scotese, C.R., Brasier, M.D. (1992). Early Cambrian continental reconstructions.  
565 *Journal of the Geological Society*, 149(4), 599-606.
- 566 Merriam, C.W., Palmer, A.R. (1964). Cambrian rocks of the Pioche mining district, Nevada, with a  
567 section on Pioche shale faunules (No. 469). *USGS Professional Paper*, 264-D, 53-86
- 568 Montañez, I.P., Osleger, D. A., Banner, J.L., Mack, L. E., Musgrove, M. (2000). Evolution of the Sr and  
569 C isotope composition of Cambrian oceans. *GSA today*, 10(5), 1-7.
- 570 Morgan, W.A. (2012). Sequence stratigraphy of the great American carbonate bank, *in*, Derby, J.R.,  
571 Fritz, R.D., Longacre, S.A., Morgan, W.A., and Sternbach, C.A., eds., *The Great American*  
572 *Carbonate Bank: The Geology and Economic Resources of the Cambrian-Ordovician Sauk*  
573 *Megasequences of Laurentia: Association of American Petroleum Geologists Memoir 98*, p.37-  
574 79.
- 575 Newell, N.D. (1972). The evolution of reefs. *Scientific American*, 226, 54-65.
- 576 Palmer, A.R., Halley, R.B. (1979). Physical stratigraphy and trilobite biostratigraphy of the Carrara  
577 Formation (Lower and Middle Cambrian) in the southern Great Basin. *USGS Professional Paper*,  
578 No.1047.
- 579 Palmer, A. R. (1984). The biomere problem: evolution of an idea. *Journal of Paleontology*, 599-611.
- 580 Palmer, A.R. (1998). Terminal early Cambrian extinction of the Olenellina: documentation from the  
581 Pioche Formation, Nevada. *Journal of Paleontology*, 72 (04), 650-672.
- 582 Payne, J.L., Lehrmann, D.J., Wei, J., Orchard, M. J., Schrag, D. P., Knoll, A.H. (2004). Large  
583 perturbations of the carbon cycle during recovery from the end-Permian  
584 extinction. *Science*, 305(5683), 506-509.
- 585 Peng, S., Babcock, L.E., Cooper, R.A. (2012). The Cambrian Period. . In: Gradstein, F., Ogg, J., Schmitz,  
586 M., Ogg, G. (Eds). *The Geologic Time Scale 2012*, Elsevier, Boston, 2, 437-488.

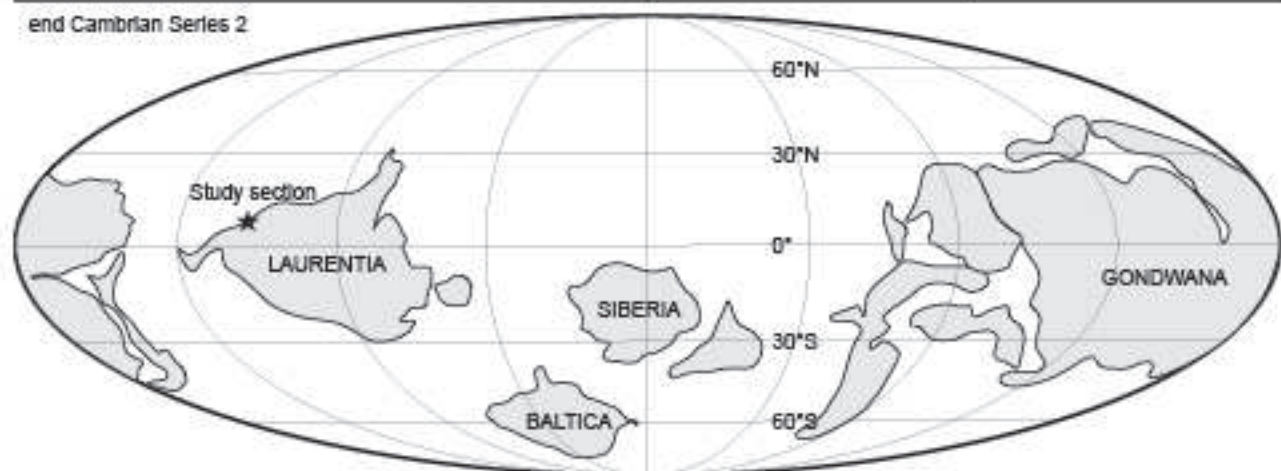
- 587 Prave, A.R. (1991). Depositional and sequence stratigraphic framework of the Lower Cambrian  
588 Zabriskie Quartzite: implications for regional correlations and the Early Cambrian  
589 paleogeography of the Death Valley region of California and Nevada. *Geological Society of*  
590 *America Bulletin*, 104(5), 505-515.
- 591 Prave, A. R. (1999). Two diamictites, two cap carbonates, two  $\delta^{13}\text{C}$  excursions, two rifts: the  
592 Neoproterozoic Kingston Peak Formation, Death Valley, California. *Geology*, 27(4), 339-342.
- 593 Pruss, S.B., Finnegan, S., Fischer, W.W., Knoll, A.H. (2010). Carbonates in skeleton-poor seas: new  
594 insights from Cambrian and Ordovician strata of Laurentia. *Palaios*, 25(2), 73-84.
- 595 Saltzman, M.R., Thomas, E. (2012). Chapter 11- Carbon isotope stratigraphy. In: Gradstein, F., Ogg, J.,  
596 Schmitz, M., Ogg, G. (Eds). *The Geologic Time Scale 2012*, Elsevier, Boston, 1, 207-232.
- 597 Saltzman, M.R., Edwards, C.T., Adrain, J.M., Westrop, S.R. (2015). Persistent oceanic anoxia and  
598 elevated extinction rates separate the Cambrian and Ordovician radiations. *Geology*, 43(9),  
599 807-810.
- 600 Sloss, L.L. (1963). Sequences in the cratonic interior of North America. Geological Society of America  
601 Bulletin, 74(2), 93-114.
- 602 Stewart, J. H. (1972). Initial deposits in the Cordilleran geosyncline: Evidence of a late Precambrian (<  
603 850 my) continental separation. *Geological Society of America Bulletin*, 83(5), 1345-1360.
- 604 Sundberg, F.A., McCollum, L.B. (2000). Ptychopariid trilobites of the lower-middle Cambrian  
605 boundary interval, Pioche Shale, southeastern Nevada. *Journal of Paleontology*, 74(4), 604-630.
- 606 Sundberg, F. A., Geyer, G., Kruse, P. D., McCollum, L. B., Pegel, T. V., Zylinska, A., Zhuravlev, A. Y.  
607 (2016). International correlation of the Cambrian Series 2 - 3, stages 4 - 5 boundary interval.  
608 *Australasian Palaeontological Memoirs*, 49, 83-124

- 609 Tarhan, L. G., Droser, M.L., Planavsky, N. J., Johnston, D.T. (2015). Protracted development of  
610 bioturbation through the early Palaeozoic Era. *Nature Geoscience*, 8, 865-869.
- 611 Wang, X., Hu, W., Yao, S., Chen, Q., Xie, X. (2011). Carbon and strontium isotopes and global  
612 correlation of Cambrian Series 2 - Series 3 carbonate rocks in the Keping area of the  
613 northwestern Tarim Basin, NW China. *Marine and Petroleum Geology*, 28(5), 992-1002.
- 614 Wignall, P.B. (2001). Large igneous provinces and mass extinctions. *Earth-Science Reviews*, 53(1), 1-  
615 33.
- 616 Wignall, P.B. (2015). *The Worst of Times: How Life on Earth Survived Eighty Million Years of*  
617 *Extinctions*. Princeton University Press.
- 618 Wilkin, R. T., Barnes, H. L., Brantley, S.L. (1996). The size distribution of framboidal pyrite in modern  
619 sediments: an indicator of redox conditions. *Geochimica et Cosmochimica Acta*, 60(20), 3897-  
620 3912.
- 621 Zhang, W., Shi, X., Jiang, G., Tang, D., Wang, X. (2013). Mass-occurrence of oncoids at the Cambrian  
622 Series 2 - Series 3 transition: Implications for microbial resurgence following an Early Cambrian  
623 extinction. *Gondwana Research*, 28(1), 432-450.
- 624 Zhu, M. Y., Zhang, J. M., Li, G. X., Yang, A. H. (2004). Evolution of C isotopes in the Cambrian of China:  
625 implications for Cambrian subdivision and trilobite mass extinctions. *Geobios*, 37(2), 287-301.
- 626 Zhu, M.Y., Babcock, L.E., Peng, S.C. (2006). Advances in Cambrian stratigraphy and paleontology:  
627 integrating correlation techniques, paleobiology, taphonomy and paleoenvironmental  
628 reconstruction. *Palaeoworld*, 15(3), 217-222.
- 629 Zhuravlev, A.Y., Wood, R. A. (1996). Anoxia as the cause of the mid-Early Cambrian (Botomian)  
630 extinction event. *Geology*, 24(4), 311-314.
- 631





end Cambrian Series 2



CARRARA FM,  
EMIGRANT  
PASS, CA

116°W



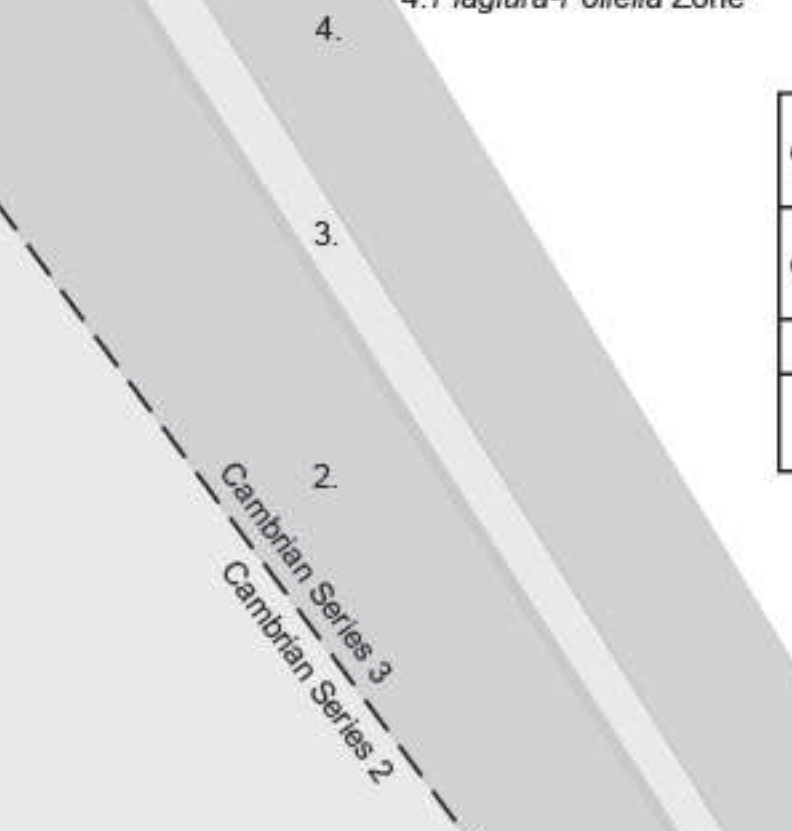
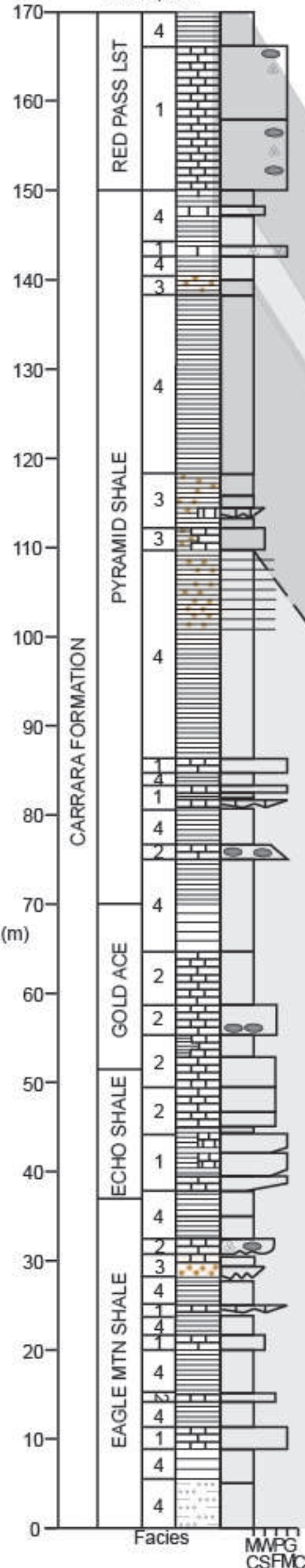
KEY



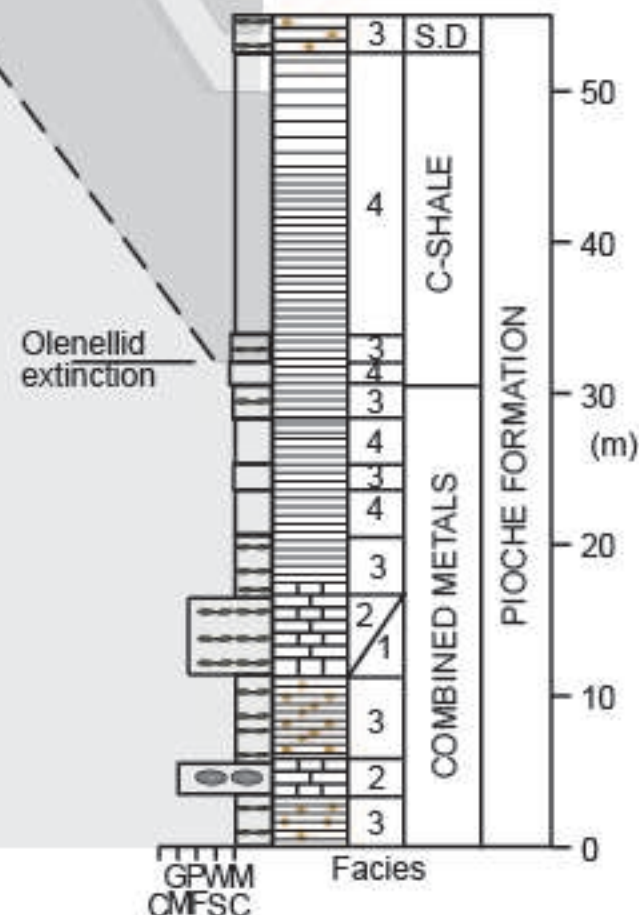
BIOZONES

1. *Olenellus* Zone
2. *Eokochaspis nodosa* Zone
3. *Amecephalus arrosensis* Zone
4. *Plagiura-Poliella* Zone

G Series 3	Bonanza King
	Carrara Fm
G Series 2	Zabriskie Quartzite
	Wood Canyon Fm
Pre G	Stirling Quartzite



PIOCHE FM,  
OAK SPRINGS  
SUMMIT, NV



Olenellid extinction

Facies

MMPG  
CSFMC

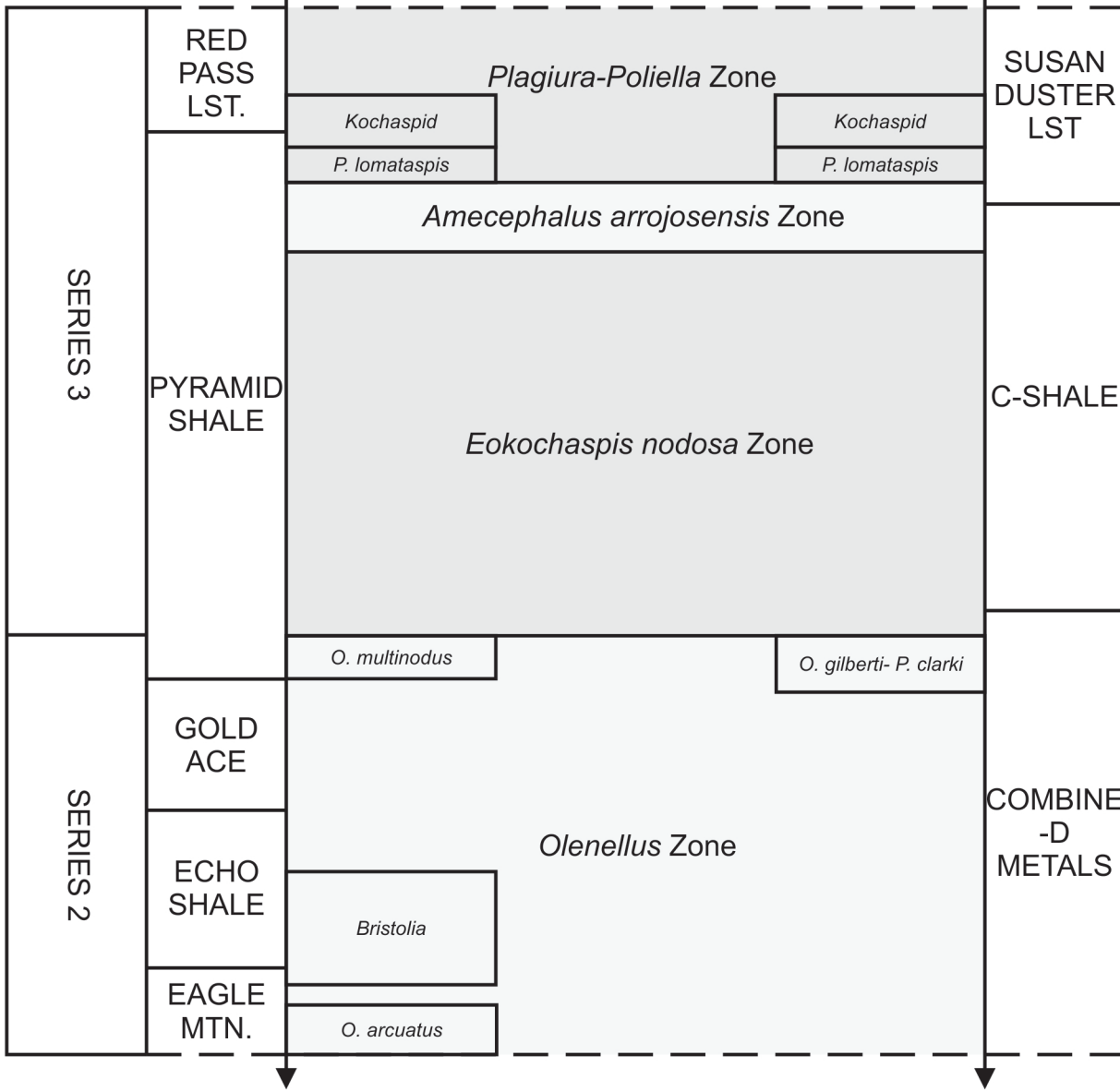
GPWM  
CMFSC

Facies

(m)

CARRARA  
FM

PIOCHE  
FM



CAMBRIAN  
SERIES

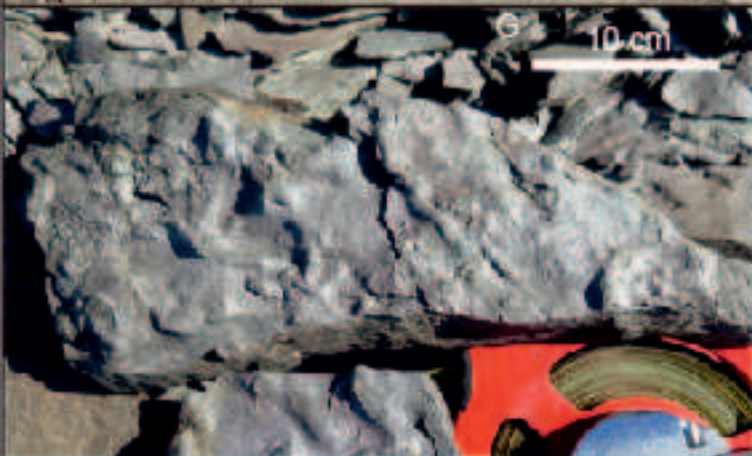
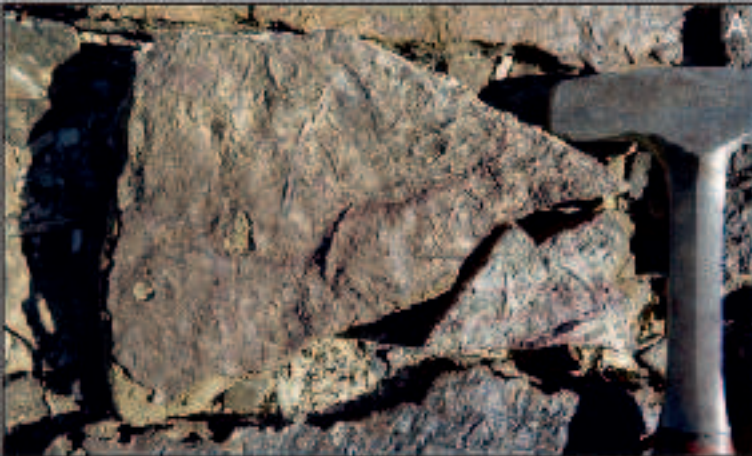
MEMBER

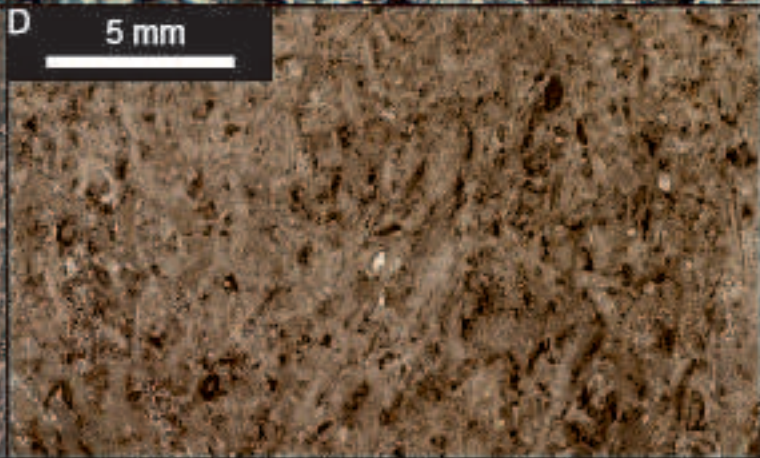
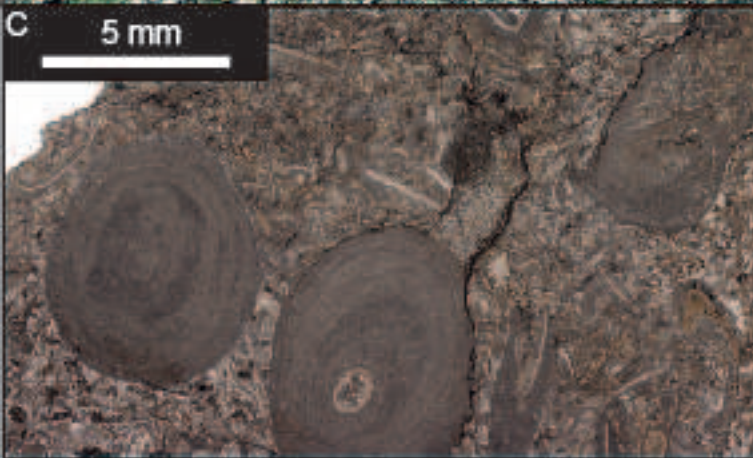
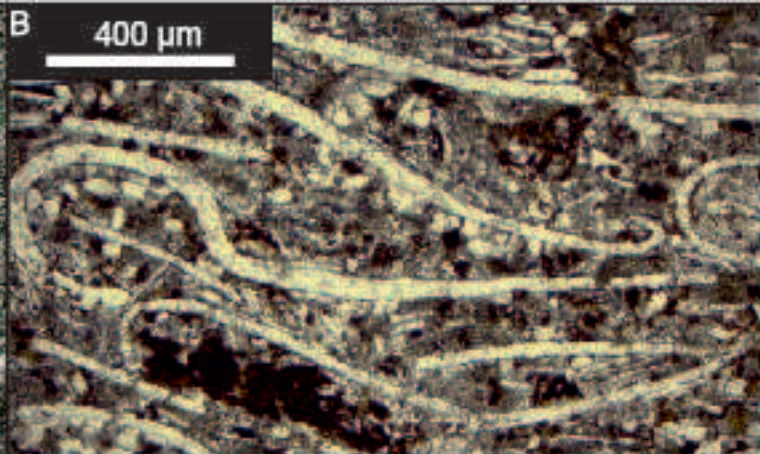
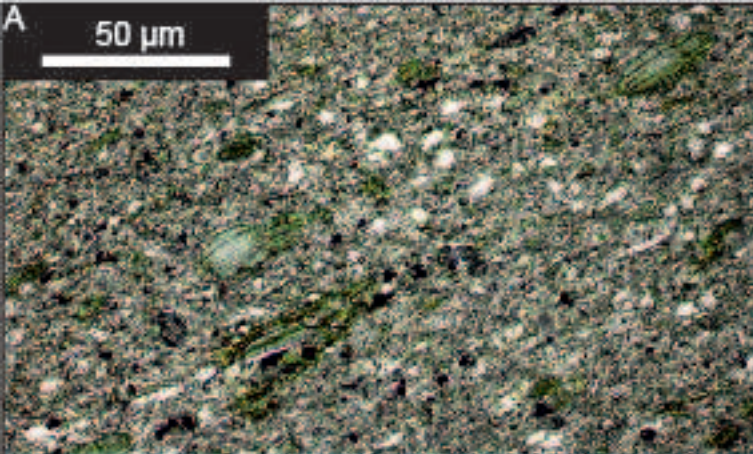
“ZONULE”

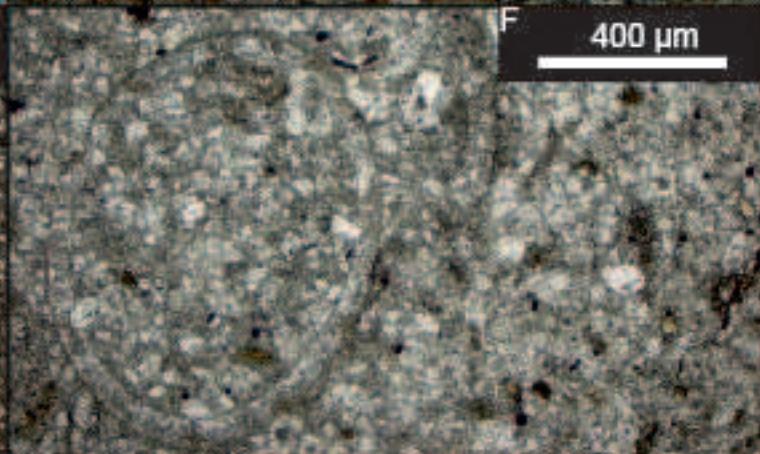
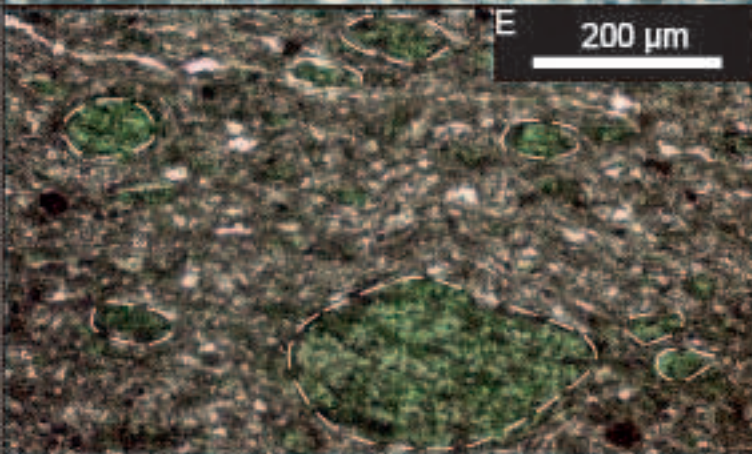
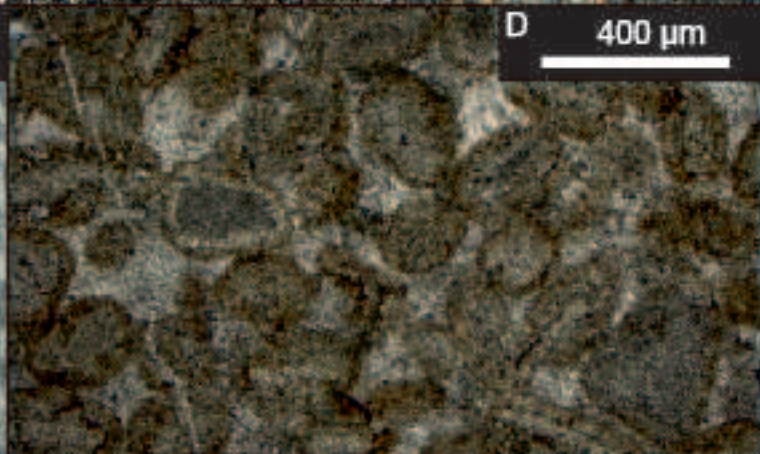
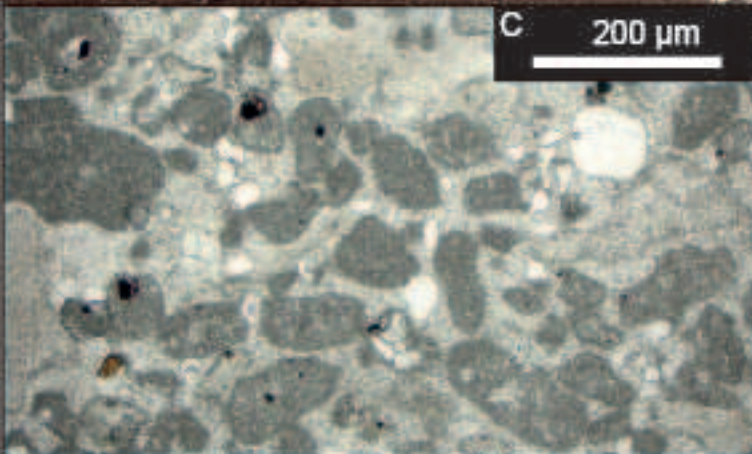
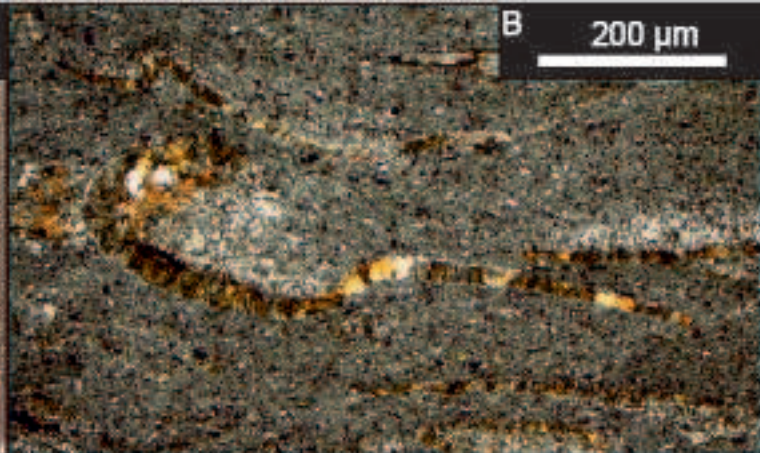
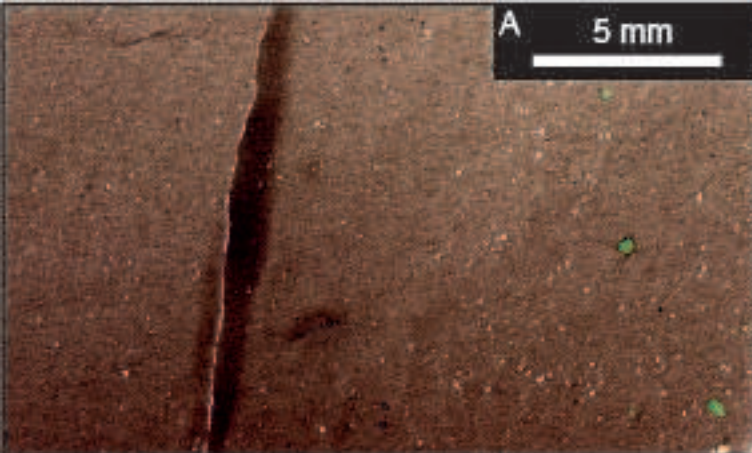
LAURENTIAN  
TRILOBITE ZONE

“ZONULE”

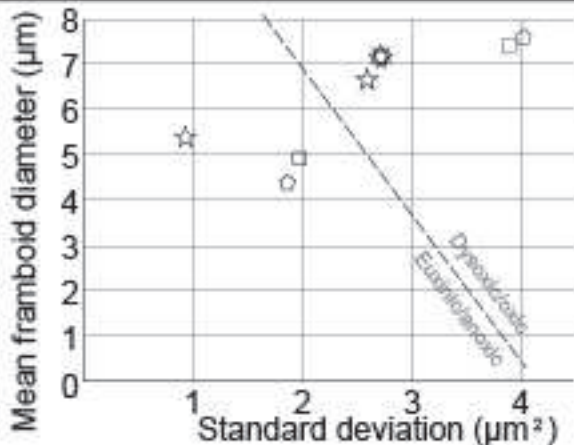
MEMBER





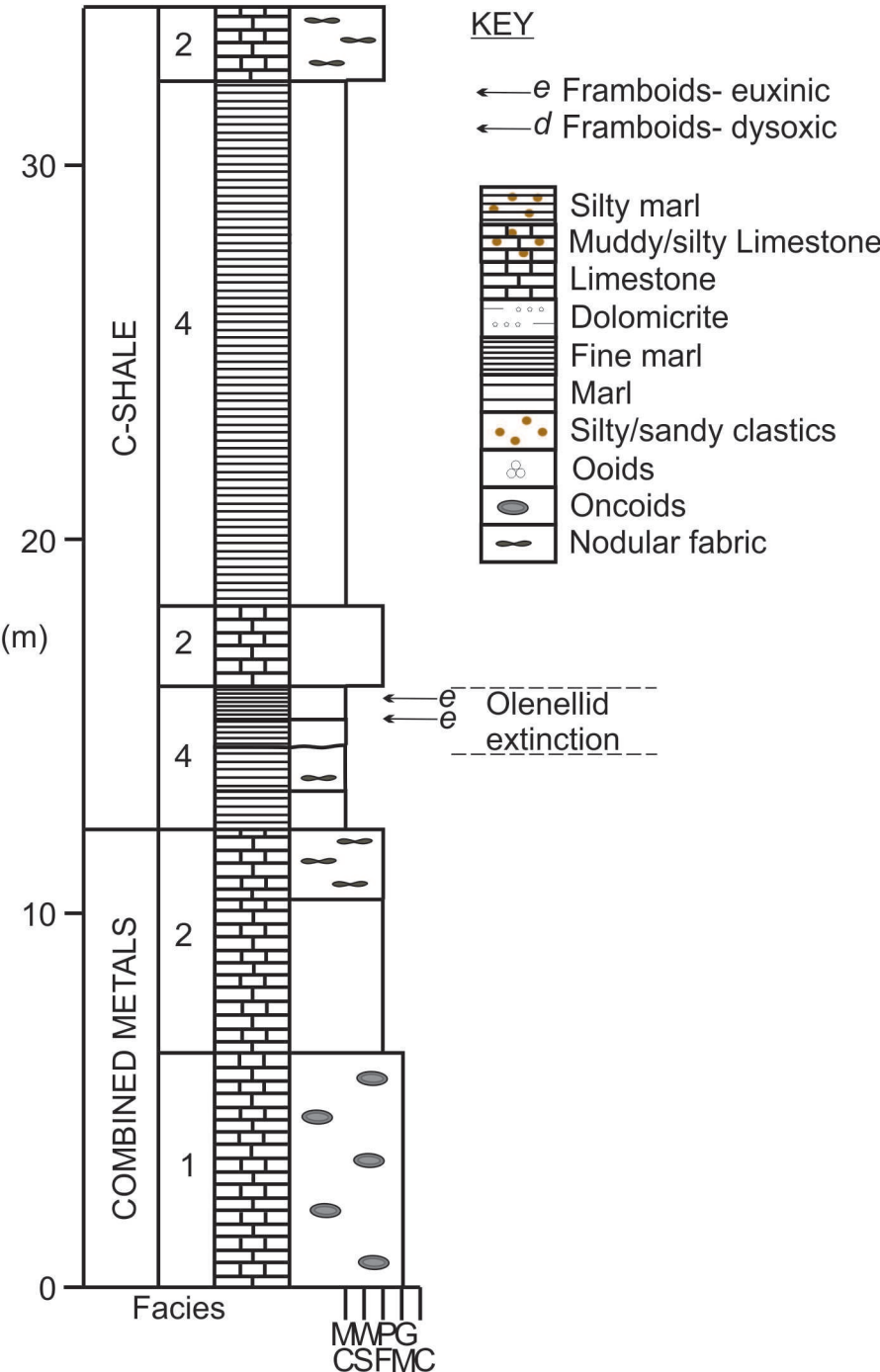




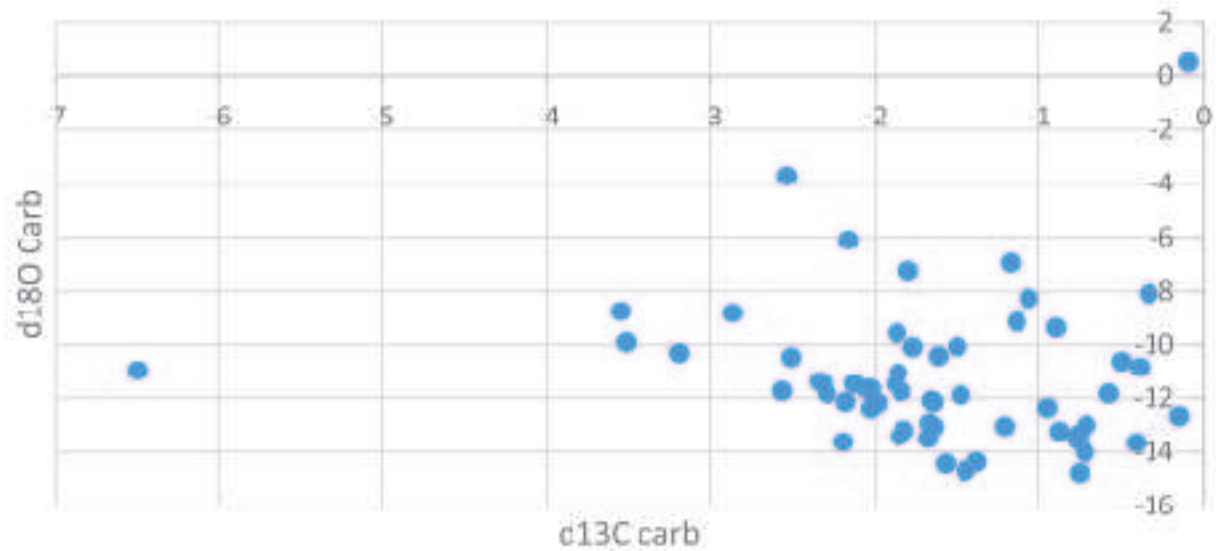


- ⚙ ☆ □ ○ Combined Metals Mbr, Oak Springs Summit
- ☆ C-Shale Mbr, Oak Springs Summit
- ○ C-Shale Mbr, Ruin Wash

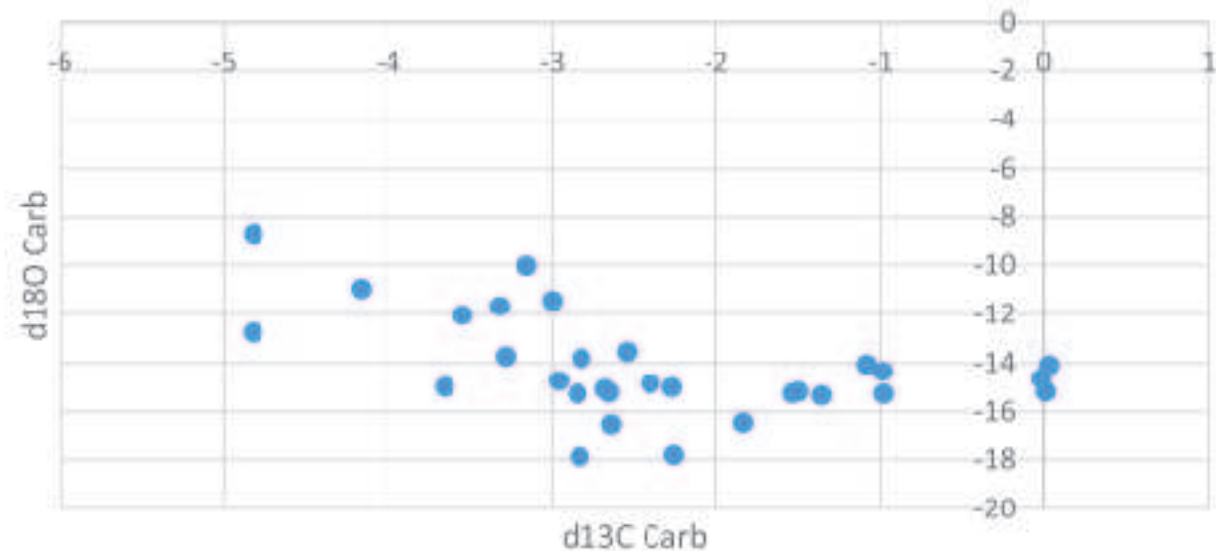
PIOCHE FM,  
 RUIN WASH,  
 NV



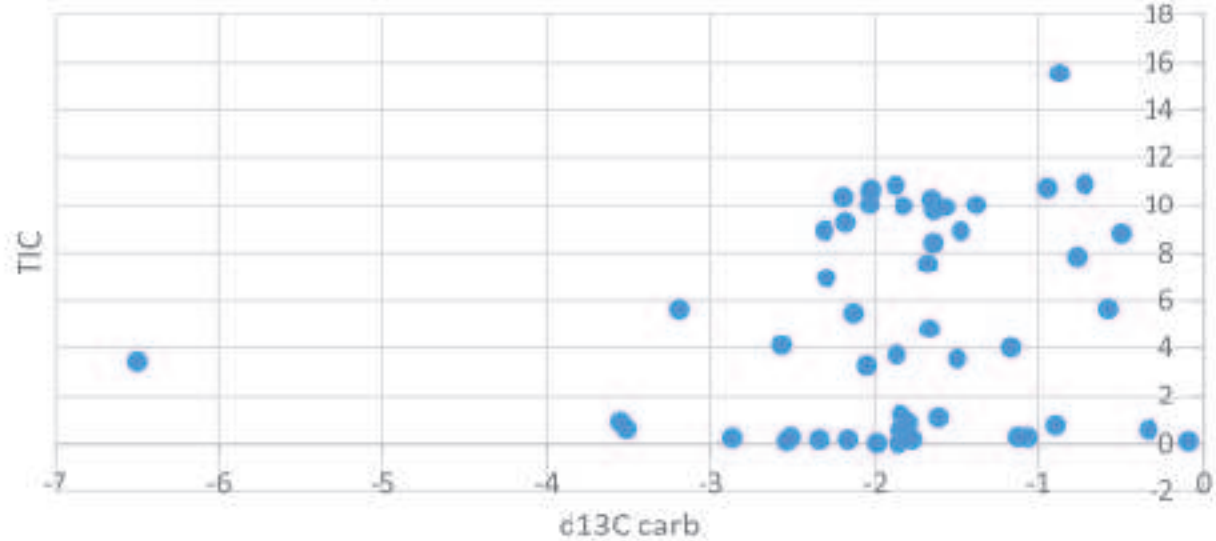
2 Carrara Formation



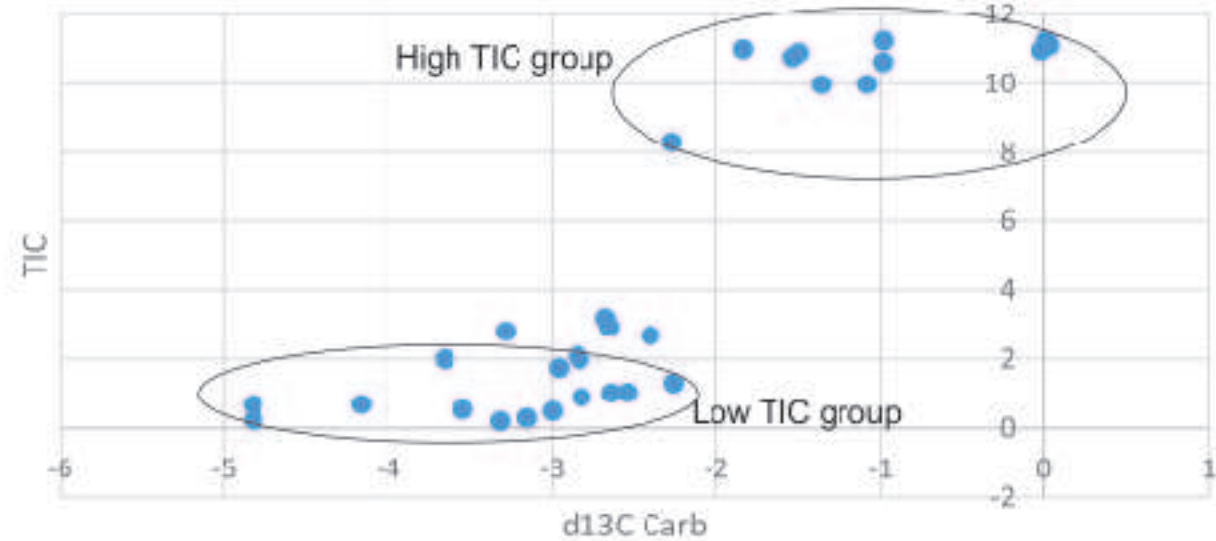
3 Pioche Formation



4 Carrara Formation



5 Pioche Formation



6 Pioche Formation

